#### **RESEARCH ARTICLE**



# Elastic nozzles reduce the influence of pressure pulses on liquid jets

MD. Emazuddin Alif<sup>1</sup> · Mackenzie Brogan<sup>1</sup> · Fellah Mohsun<sup>1</sup> · Christopher Williamson<sup>1</sup> · Reagan Barr<sup>1</sup> · Ria Corder<sup>2</sup> · Andrew K. Dickerson<sup>1</sup>

Received: 11 March 2025 / Revised: 13 August 2025 / Accepted: 14 August 2025 © The Author(s), under exclusive licence to Springer-Verlag GmbH Germany, part of Springer Nature 2025

#### **Abstract**

Nozzle characteristics modulate the stability of liquid jets, but their role in jet robustness to external disturbances is understudied. Here we produce jets with thin elastic membranes containing a hole of approximately 500  $\mu$ m in undeformed diameter. Our softest membranes produce the most stable jets in the Rayleigh and first wind-induced breakup regimes. An externally applied upstream pressure pulse lasting approximately 1 ms momentarily reduces the jet breakup distance and alters morphology. The pressure pulse is generated by the strike of a coil spring against a membrane mounted to the jet relaxation chamber. Softer nozzles and higher jet velocities minimize the disruption to the otherwise steady jet. Linear temporal theory for short nozzles derived using a dilated nozzle diameter well predicts breakup length before and after the pressure pulse. We propose hypothetical states for which our pressure pulse does not affect jet stability. Pressure disturbances initiate morphological changes in the jet, introducing novel phenomena like jet thinning and exit coalescence. Our results demonstrate that nozzle compliance can play a significant role in damping undesirable disturbances.

#### 1 Introduction

Liquid jets play a critical role in a wide range of processes (Jarrahbashi and Sirignano 2012; Mitragotri 2006; Reneker et al. 2000), such as cleaning of foulants (Guha et al. 2011; Krsmanovic et al. 2021), inkjet printing (Furlani et al. 2006), chemical synthesis (Zhang et al. 2007), drug delivery (Menezes et al. 2009; Tagawa et al. 2013), and microfabrication (MacFarlane et al. 1994; Carter et al. 2006). Mathematical models (Amini et al. 2014; Eggers and Villermaux 2008; Ashgriz and Yarin 2011; Sirignano and Mehring 2000; Entov and Yarin 1984, 1980; Smith et al. 2018) to describe liquid jet characteristics span nearly two centuries (Savart 1833; Bidone 1829; Rayleigh 1879, 1878). The stability of liquid jets, as characterized by the length of the coherent liquid column Z, is dependent on various factors, including but not limited to surface tension  $\sigma$ , ambient pressure, jet exit velocity  $V_0$ , viscosity of liquid  $\mu$ , density ratio between liquid and gas  $\rho/\rho_{\rm G}$ , and turbulence at the nozzle (Eggers and Villermaux 2008; Sirignano and Mehring 2000; Lin and Reitz 1998; Ohnesorge 1936). The forces acting on the surface of the jet grow as the liquid moves downstream to induce breakup (Ashgriz 2011; Eggers and Villermaux 2008).

Liquid jets undergo four breakup regimes (Eggers and Villermaux 2008; Sirignano and Mehring 2000; Lin and Reitz 1998; Ohnesorge 1936) based on their liquid and gas Weber numbers We =  $\rho V_0^2 D/\sigma$  and We<sub>G</sub> =  $\rho_G V_0^2 D/\sigma$ , respectively, where D is the diameter of a circular jet. We investigate jets in the Rayleigh and the first wind-induced breakup regimes. The Rayleigh regime begins following the transition from dripping to jetting, at We > 8 and  $We_G < 0.4$ . In this regime, the aerodynamic interactions with ambient gas are not significant, and as such, the dominant forces inducing breakup are the capillary forces pinching inward and the growth of long-wavelength, smallamplitude disturbances on the surface. The disturbances are axisymmetric, and the droplets generated have a radius in the same order of the jet radius (Sirignano and Mehring 2000). Gas inertia becomes dominant in the first wind-induced breakup regime (Ranz 1956) at  $0.4 < We_G < 13$ , where a jet from a traditionally rigid nozzle reaches its maximum length (Etzold et al. 2018; Sterling and Sleicher 1975; Sirignano and Mehring 2000). Oscillations in this regime include non-axisymmetric components, but the droplets

Published online: 05 September 2025



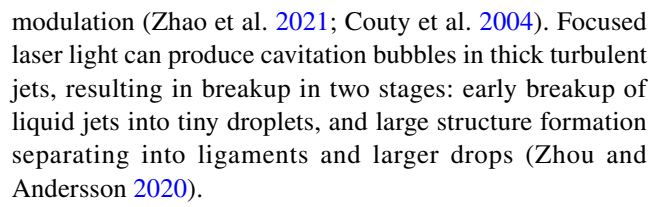
Andrew K. Dickerson

Mechanical, Aerospace, and Biomedical Engineering, University of Tennessee, Knoxville, USA

Chemical and Biomolecular Engineering, University of Tennessee, Knoxville, USA

produced are still on the same order of magnitude as the jet radius. At greater We, jets enter the second wind-induced (13 < We $_{\rm G}$  < 40.3) and atomization (We $_{\rm G}$  > 40.3) regimes, where the jet stability decreases with increasing We (Lin and Reitz 1998).

Significant research has been conducted to control the breakup distance and directionality of liquid jets through capillary breakup (Rayleigh 1878), co-flowing gases (Gañán-Calvo and Barrero 1999; Varga et al. 2003), passive inlet conditions and nozzle geometry, (Rajesh et al. 2016; Lefebvre and McDonell 2017; Song et al. 2017; Blaisot and Adeline 2003; Amini and Dolatabadi 2011; Ghassemieh et al. 2006; Amini et al. 2014; Wang and Fang 2015), dilating nozzles (Alif et al. 2023), laser-induced breakup (Couty et al. 2004; Zhou and Andersson 2020; Zhao et al. 2021), and external forcing (Amini and Dolatabadi 2012; Kalaaji et al. 2003). Prior works have investigated jets interacting with external disturbances induced by nozzle geometry (Ghassemieh et al. 2006; Wang and Fang 2015; Alif et al. 2022), pulsed lasers(Couty et al. 2004; Zhou and Andersson 2020; Zhao et al. 2021), and co-flowing gases (Chigier and Farago 1992; Chigier 1996; Eroglu et al. 1991). Ghassemieh (2006) studied the discharge and velocity coefficients of 120-170-µm diameter conical, cone-capillary, and multihole nozzles used in various industrial and manufacturing processes(Ghassemieh et al. 2006). Cavitation effects due to rapid local changes in pressure dominate the characteristics of such small nozzles. Rounded and conical inlets with small cone angles generate smooth flow attached to the nozzle, whereas flow separates for sharp inlets and high cone angles. Manufacturing tolerances and surface roughness effects become critically important factors in determining flow characteristics of very small nozzles (Ghassemieh et al. 2006). Wang (2015) observed axis switching in rectangular nozzles, and more ambient gas interactions for square and triangular nozzles (Wang and Fang 2015). Noncircular nozzles have more instabilities at high-velocity regimes compared to circular nozzles. High-velocity gas flow around a liquid jet transmits momentum onto the jet surface and causes additional breakup regimes beyond the traditional four (Chigier 1996). The impact of large-scale eddy structures of the co-flowing gas on the jet results in stretching, destabilization, and flapping of the jet (Lin and Reitz 1998). The stability of liquid jet decreases with increasing liquid We and increases with increasing gas Reynolds number Re =  $\rho_G V_0 D / \mu_G$ , where  $\mu_G$  is the gas viscosity (Eroglu et al. 1991; Chigier and Farago 1992; Chigier 1996). External pulsed lasers also introduce surface disturbances of liquid jets. In such cases, jet breakup is controlled by the competition between the growth of the initial disturbances resulting in Rayleigh-Plateau instabilities and the disturbances caused by surface tension perturbations from pulsed heating-induced temperature



In a previous study (Alif et al. 2023), we investigated liquid jet stability through elastic planar membranes and modified the linear temporal theory of free jets to account for dilating nozzles. Our modified linear temporal theory shows that normalized jet stability,  $Z/D_0 \sim We^{1/2} \check{D}$ , where  $\check{D} = D/D_0$  is nozzle dilation and  $D_0$  is the initial diameter of the nozzle. Softer nozzles show greater  $\check{D}$  and  $Z/D_0$ . The breakup length of a planar rigid nozzle is less than that of short tapered nozzles of similar diameter studied by Etzold et al. (2018) Etzold et al. (2018). Gradual flow contraction mitigates the instabilities associated with rounding sharp corners. In this study, we use a slightly modified experimental setup to investigate the role of dilating planar nozzles in damping upstream pressure pulses in lowvelocity regimes in an attempt to discover a passive means to make liquid jets more robust to external disturbances. The  $\sim$  1-ms pressure pulse reduces the breakup distance and introduces temporary morphological changes in the liquid jet, as shown in Fig. 1. The material properties of the dilating nozzle modulate the degree of such influence on the jets. We measure the dilation and the breakup distance of the coherent jet before and as the pulse is applied. Nozzles begin approximately as 500-µm-diameter circles but can sometimes produce jets  $> 1600 \mu m$  in diameter.

#### 2 Methods

Silicone rubber elastomer sheets of shore hardness 10A, 20A, and 35A and thickness of 0.51 mm (0.2 in) are sourced from McMaster-Carr. A 500-µm circular punch makes holes for nozzles in our membranes. Elastic moduli of the membranes are calculated by Larson (2016)  $\log_{10} E = 0.0235S - 0.6403$ , where S = 35, 20, 10 is the shore A hardness. Our elastomers have relaxation times ranging from 199 – 456 s, measured by a TA instruments HR-20 rheometer and fit to a discrete stress relaxation model with four Maxwell elements. Since the timescale of our experiments is less than the relaxation time, we anticipate no change in the effective modulus during a trial. A control nozzle is cut out of 0.51-mm-thick high-strength 2024 aluminum sheet with a pulsed laser. The initial diameter  $D_0$  of all nozzles is measured with a Keyence VHX-7000 digital microscope and listed in Table 1 along with pertinent material properties.

Water is delivered to the relaxation chamber from a pressurized soda keg, as depicted in Fig. 2. The flow rate is controlled by a ball valve and measured with Micro-Flo



Experiments in Fluids (2025) 66:176 Page 3 of 11 176

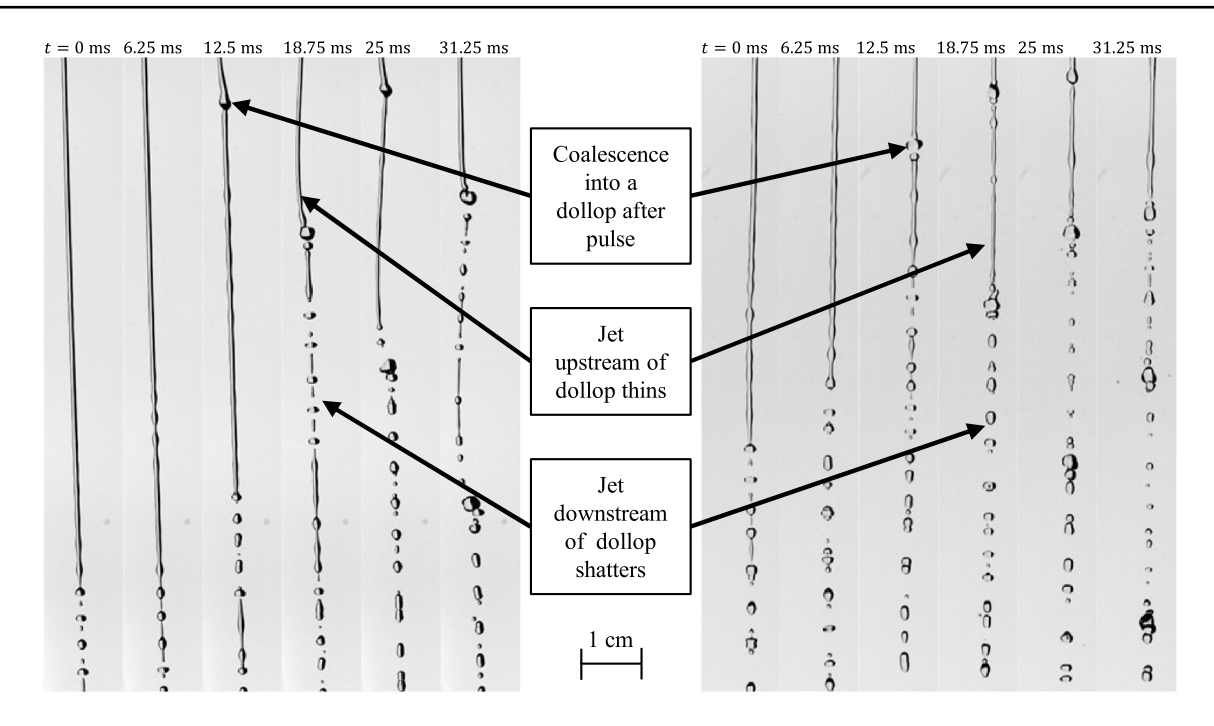
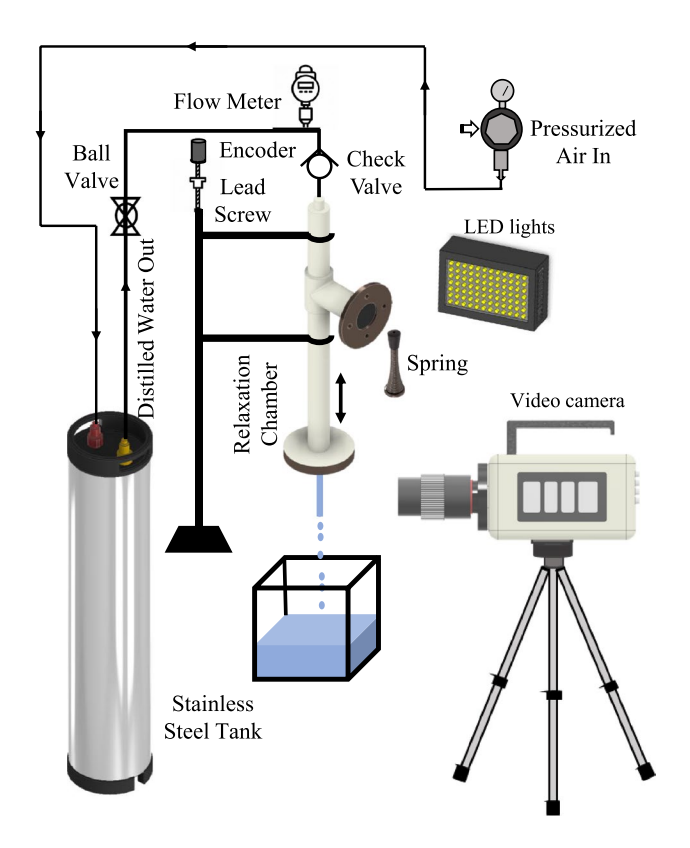


Fig. 1 Photographic depictions of jet temporal breakup for membrane 10A (left, E = 0.4 MPa) and 20A (right, E = 0.7 MPa) at 150 mL/min. Pressure pulse reduces breakup distance and induces morphological changes in the jet. Multimedia available online



**Fig. 2** Experimental setup of jet stability through deformable nozzles. A pressure pulse is applied at the T-fitting with a spring

**Table 1** Experimental material thickness h, estimated modulus E, and nominal nozzle diameter  $D_0$ . Materials are listed in order of decreasing shore hardness

Material	35A	20A	10A
h [μm]	508	508	508
E [MPa]	1.5	0.7	0.4
$D_0 [\mu \mathrm{m}]$	536	535	478
Re	2482 - 8030	2536 - 7402	2950 - 6343
We	24 - 498	90 - 472	117 - 430
$We_G$	0.10 - 0.60	0.11 - 0.83	0.14 - 0.52

FS1-201-6V digital paddlewheel flow meter. The relaxation chamber is mounted on a linear stage affixed to a 4×10 ft Coherent optical table vibration isolated by pneumatic legs. A Yumo E5A2-CW3C quadrature rotary encoder records the vertical displacement of the relaxation chamber mounted to a linear stage. An Arduino Uno records displacement at a resolution of 0.025 mm. The relaxation chamber is 41 cm long and 2.54 cm in diameter, with a 1-inch PVC T fitting placed 4.5 inches above the top. Internal aramid laminarizers before and after the T-fitting straighten the flow. The T-fitting terminates with a galvanized iron flange and an acrylic ring clamping a watertight fabric membrane. A coil spring doorstop is pulled back against a string and released to strike the fabric, much like a mallet striking a drum, to provide a repeatable impulsive force with a maximum amplitude of  $17 \pm 0.95$  N (N = 10). The mallet remains in contact with



176 Page 4 of 11 Experiments in Fluids (2025) 66:176

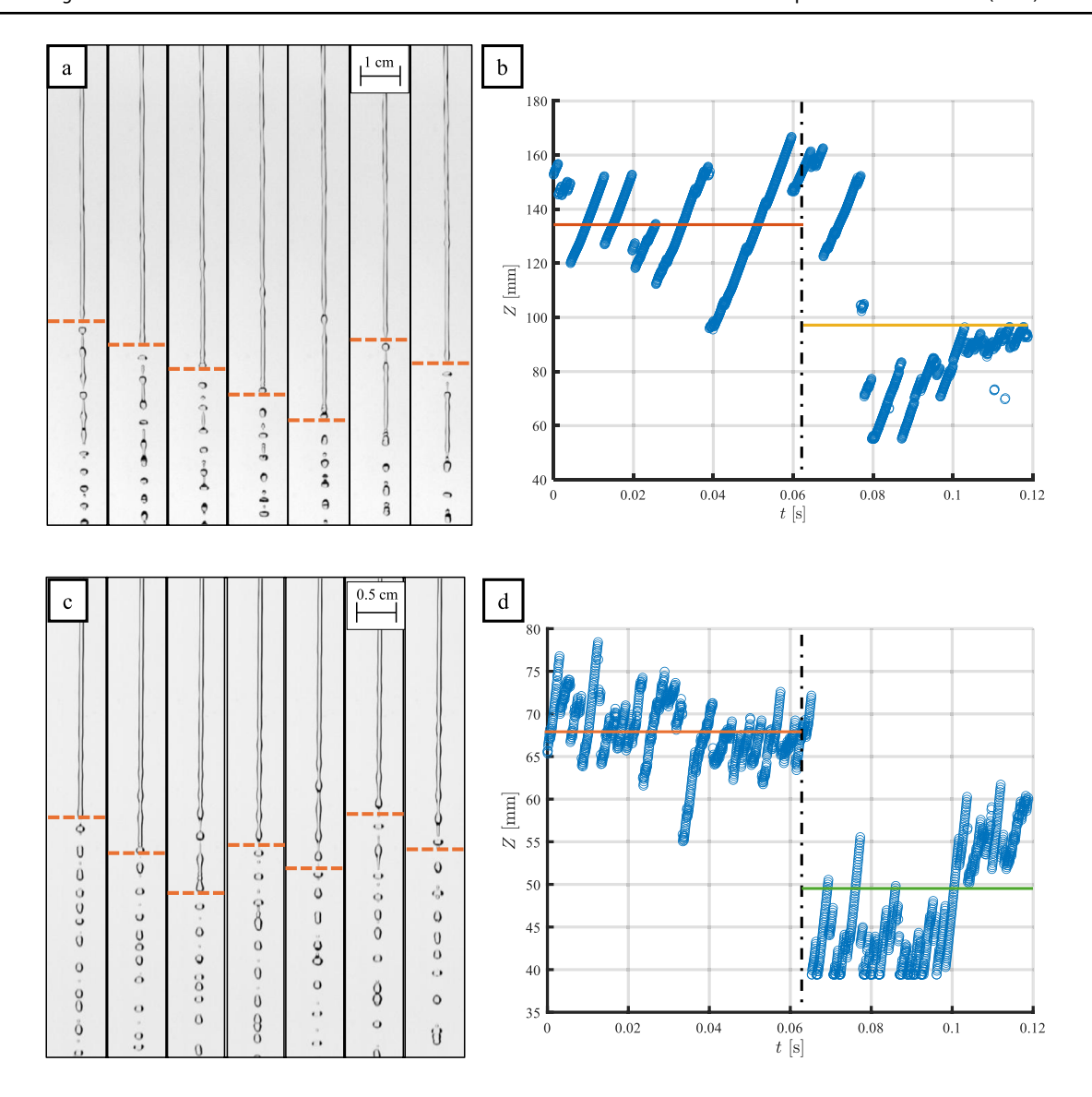


**Fig. 3** Representative temporal breakup for soft 10A and rigid aluminum nozzles. (a) and (c) Coherent jets flow vertically downward after breaking up. The next breakup event happens upstream at a distance similar to the prior breakup event. The time between

photographs is 1.6ms. (b) and (d) Breakup length Z vs time t. The vertical line indicates the application of the pulse. Horizontal lines indicate the average Z before and after the pulse

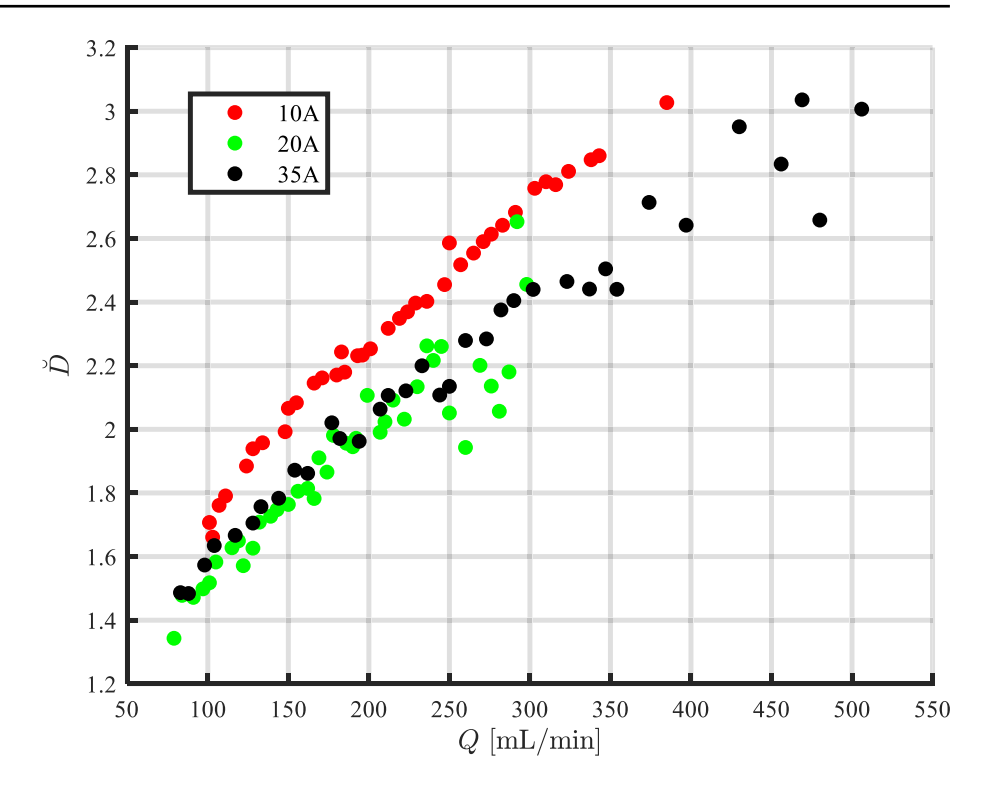
the membrane for  $1.1 \pm 0.2$  ms (N = 5), measured visually. We measured the maximum impulsive force with a Mark-10 Series 5 M51 force gauge and the pulse length from high-speed videos. We visualize the pulse by recording its sound via a Shure MV5 microphone. A normalized sound pressure intensity plot is provided in Fig. S1. A check valve on the incoming water line limits the backflow caused by the spring-induced pressure pulse. The nozzle membranes are sandwiched in a configuration similar to that of the fabric that adorns the T fitting. The nozzle flange has an inner diameter of 2.4 cm, and the diameter of the drumhead (i.e., the portion of the nozzle allowed to expand) is 1.78 cm.

We capture videos of jets in equilibrium for each flow rate before the spring-induced pulse is applied. During the prepulse period, we measure jet diameter D by time averaging the diameter of the first  $\sim 2$  cm of the steady jet from the nozzle exit, a spatial zone devoid of visible Rayleigh–Plateau instabilities. A Photron FASTCAM Nova S6 fitted with a Nikon Micro-NIKKOR 55 mm f/2.8 lens records jet breakup for 118.75 ms at 16,000 fps. The video length is limited by the second strike of a rebounding spring. The linear stage is adjusted such that the portion of the jet undergoing breakup appears in frame. Jets are backlit by custom-built LED lights such that jets appear black on a light background. Highspeed videos are binarized in MATLAB.



Experiments in Fluids (2025) 66:176 Page 5 of 11 176

**Fig. 4** Nozzle dilation  $\check{D}$  versus Reynolds number for experimental materials before the application of the pressure pulse



#### 3 Results

## 3.1 Jet breakup is spatially variant

Traditionally, jet breakup length is defined as the length of a coherent jet before breaking up into droplets and is discussed as invariant in time for fixed jetting conditions(Etzold et al. 2018). However, our observations challenge the existing notion of breakup distance Z. Representative time sequences of two sequential breakup events for soft 10A and rigid aluminum nozzles are pictured in Fig. 3a and c. After a breakup event, we observe that the coherent jet extends downward before again pinching off upstream. Between two breakup events, the length of the coherent jet, the breakup distance, increases. Therefore, the temporal measure of the breakup length manifests itself as a discontinuous function before and after the pulse, as shown in Fig. 3b and d. For the sake of comparing the breakup distance across various nozzle conditions and flow rates, we seek a single value of Z that characterizes a trial. We therefore take the time average of the instantaneous breakup distance. The calculated value of Z before and after the pressure pulse in Fig. 3b is 134 mm and 97 mm, respectively, and in Fig. 3d is 67.4 mm and 48.7 mm, respectively. For both cases, the pulse is applied at 62.5 ms. The pulse response of the jet is unseen by our camera 6 - 25 ms from the application of the pulse, a range that exists due to various jet speeds at the nozzle pushing the disturbance into view of the camera. Such a shortening of Z represents a ubiquity in our observations of the effect of our spring-induced pulse.

#### 3.2 Pressure pulses reduce jet stability

Our previous study shows that softer nozzles experience greater dilation (Alif et al. 2023). We stretch the boundaries of that prior work by investigating nozzle dilation of membranes that are less stiff and thicker. Here, we fix the membrane thickness to provide a more direct comparison of elasticity effects. Pressure-driven flow (Fig. 2) causes all of our soft membranes to strain radially outward. Nozzles expand more than  $3\times$  their initial diameter  $D_0$ . Our observations show that nozzle dilation  $\check{D} = D/D_0$  scales linearly with flow rate Q, shown in Fig. 4 for unpulsed flow and also observed in our previous study. The relation  $Q \sim \tilde{D}$  imposes a nonlinear relation between the observed jet velocity and an imposed flow rate. We observe that softer membranes experience greater dilation and the softest nozzle, i.e., 10A, dilates the most at all Q. 20-A and 35-A nozzles show very similar dilation behavior.

Our previous study modifies the linear temporal theory of breakup in the Rayleigh and the first wind-induced regimes to account for nozzle dilation, and we form a concise scaling relationship (Alif et al. 2023),

$$Z/D_0 \sim We^{1/2}\check{D},\tag{1}$$



176 Page 6 of 11 Experiments in Fluids (2025) 66:176

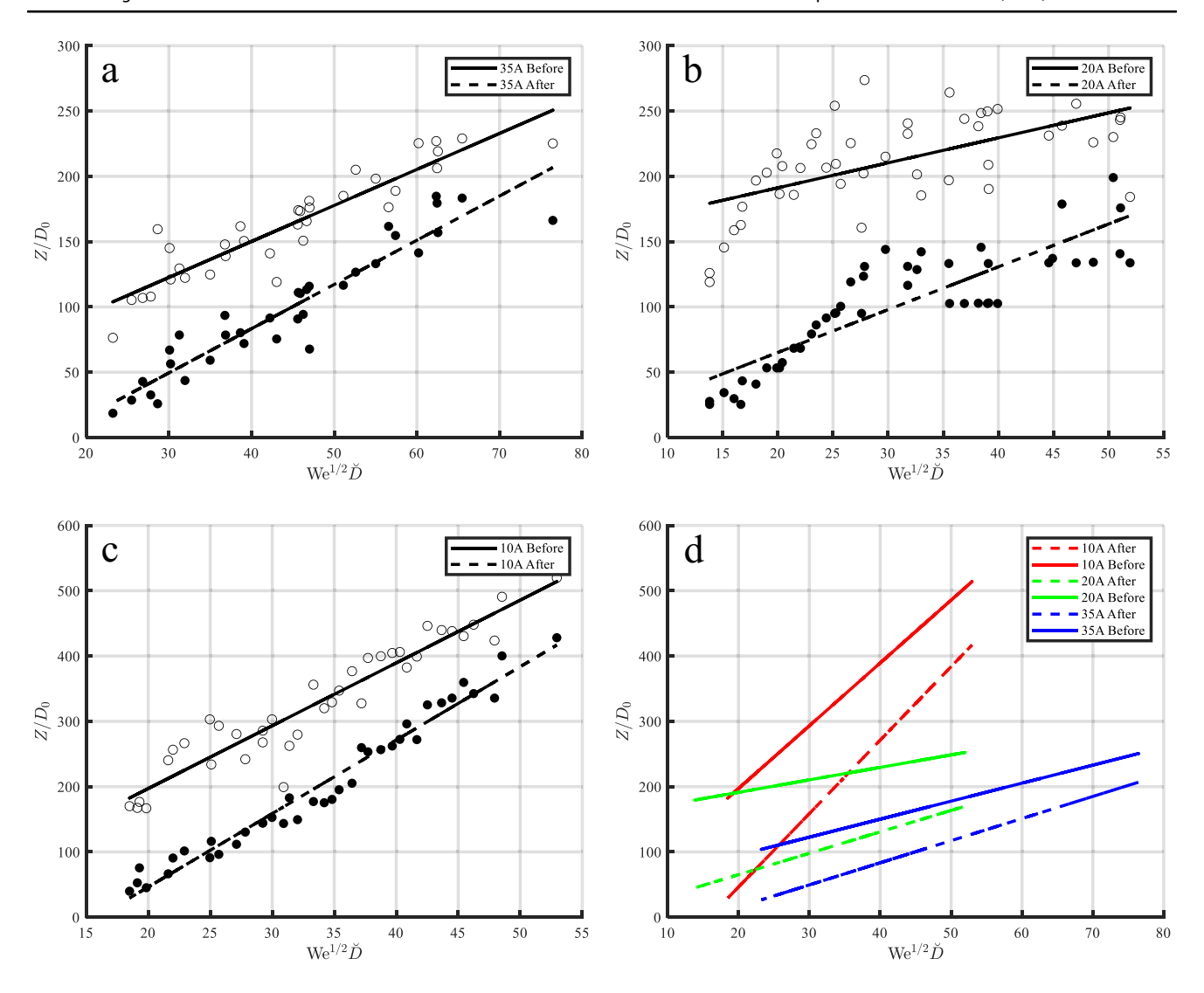


**Fig. 5** Stability curves for experimental materials (a) 35A (b) 20A, and (c) 10A. Lines correspond to the scaling relation predicted by Eq.(1). (d) Experimental stability curves for all materials before

and after the external pressure pulse. The influence of the pulse on breakup distance is lower at higher flow rates

**Table 2** Goodness of fit and predicted states for the convergence of pre- and post-pulse breakup lengths. Materials are lists in order of decreasing functional stiffness

	35A	20A	10A
Q [mL/min]	1038	850	844
$\mathrm{We}^{1/2} \check{D}$	146	112	112
R <sup>2</sup> , Eq.(1) pre-pulse	0.8447	0.3653	0.8960
R <sup>2</sup> , Eq.(1) post-pulse	0.8907	0.7453	0.9678

where We =  $\rho V_0^2 D/\sigma$  is the Weber number, such that  $V_0$  is the jet exit velocity and  $\rho$  and  $\sigma$  are the density and surface tension of the liquid, respectively. A detailed derivation of Eq.(1) is provided in Supplemental appendix. From Eq.(1),

we generally expect *Z* to increase with dilating nozzles and faster jets. Liquid jets respond to the upstream pressure pulse by reducing their breakup distance. At each flow rate, we compare the time-averaged breakup distance before application of the pulse and the instantaneous minimum breakup distance of the jet during the pulse response. Breakup distance before the pulse is averaged over 62.5ms, or 1000 frames. Jets from rigid planar nozzles are more prone to noise and disturbances on the jet surface than elastic nozzles, due to disruptions introduced by rounding a sharp corner(Alif et al. 2023).

We fit Eq.(1) to the breakup data in Fig. 5a-c for all test materials. For the three elastic nozzles, Eq.(1) characterizes jet stability during the pulse response, with  $R^2 = 0.74 - 0.96$ , listed in Table 2. A comparison of Eq.(1) fits for all materials, where the length of curves



Experiments in Fluids (2025) 66:176 Page 7 of 11 176

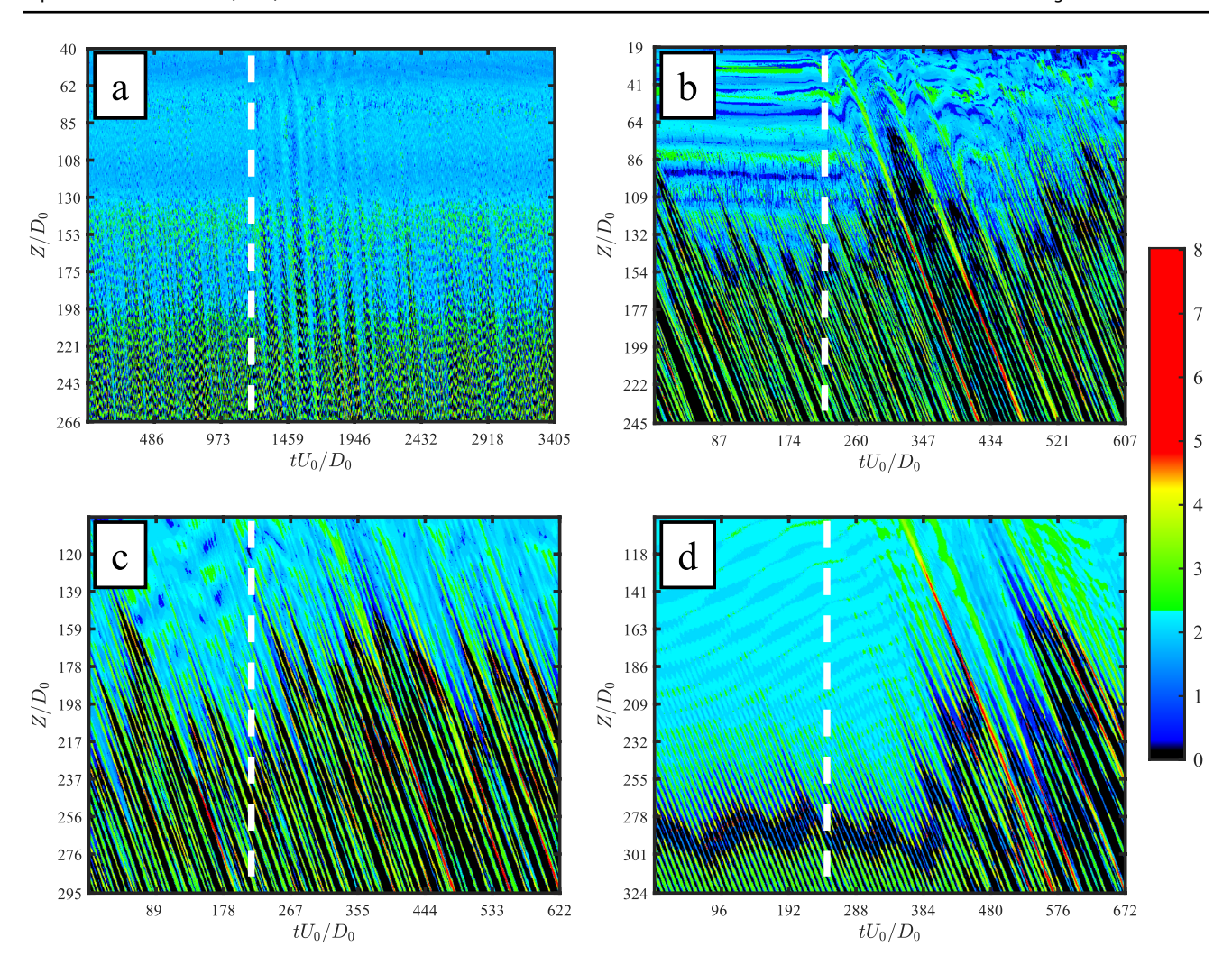


Fig. 6 Spatiotemporal diagrams for (a) aluminum, (b) 35A, (c) 20A, and (d) 10A at Q = 200 mL/min. The pressure pulse is applied at t = 31.25 ms. Color bar represents instantaneous localized jet width normalized over  $D_0$ .

demonstrates the range of We<sup>1/2</sup> $\check{D}$  we can generate for each material, is plotted in Fig. 5d. Membrane failure constrains the maximum flow rate we can test. The softest nozzle 10A produces the most stable jets for a fixed We<sup>1/2</sup> $\check{D}$ . A dimensional alternative to the plots in Fig. 5 is given in Fig. S2.

Equation (1) fits for each membrane before and after the pulse are not parallel, indicating that the pulse does not have the same influence at all flow rates. Higher flow rates minimize disruptions to a steady jet, so we predict the before and after pulse fits will converge beyond the axes limits in Fig. 5. The extrapolated intersection of the two fits defines a hypothetical state where the jet is robust to external disturbances of a similar nature to our pulse. We find a flow rate and its associated  $We^{1/2}\check{D}$  values for such a hypothetical state and list them in Table 2. Softer nozzles

damp disturbances more quickly and produce more robust jets.

Attempts to construct straight short nozzles from stock aluminum sheets of the same thickness as our soft membranes fail. Laser cutting and hole punches result in nozzles with mismatched inlets and outlets, which play a significant role in jet stability. Due to such discrepancies in shape compared to soft nozzles, we do not include aluminum nozzles in Fig. 5.

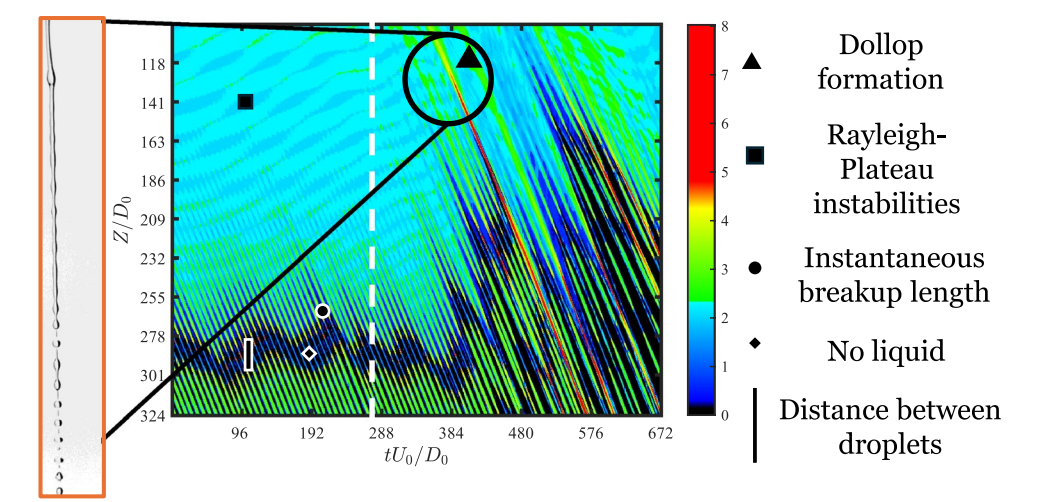
# 3.3 Pressure pulses temporarily alter jet morphology

Under the influence of an upstream pressure pulse, the breakup length of the jet cannot change independently of its morphology. A time sequence of the change in jet morphology is pictured in Fig. 1. The pulse travels from its



176 Page 8 of 11 Experiments in Fluids (2025) 66:176

**Fig. 7** Spatiotemporal diagram for 10A at Q = 200 mL/min. Features are annotated on the right



source to the nozzle exit, momentarily forcing more liquid through the nozzle to create what appears as a dollop of liquid, labeled in Fig. 1 and shown in Movie S1. The dollop is up to 2× the dilated diameter of the jet. Mass conservation dictates that the portion of the jet following the dollop is about 0.5× thinner than the diameter of the pre-pulse jet. The portion of the jet being trailed by the dollop is likewise affected by the pulse. While long filaments post-breakup are not an uncommon sight for stable jets (Alif et al. 2023), the filaments shatter in pulse-induced breakup, as shown in Fig. 1 and Movie S1.

Representative trials of aluminum, 35-A, 20-A, and 10-A membranes at  $Q \approx 200$  mL/min are used to construct spatiotemporal diagrams (STDs), shown in Fig. 6. The choice of this flow rate is done so that we can compare breakups across nozzles within the Rayleigh breakup regime. STDs are created from the binarized video frames of a jetting event, following the method detailed in Schoppink et al. (2023)Schoppink et al. (2023). The binary matrix for a frame is summed along each row, resulting in a column vector with a range of localized jet diameters. Column vectors for each frame are compiled next to one another to form the STD in y, which is an  $i \times j$  matrix, where i is the number of y-pixels in the field of view and j is the number of video frames. Jet diameters are normalized within each image by their respective  $D_0$ . STDs provide a convenient means to view the breakup behavior of an entire video in a single image, including information about the breakup that is difficult to ascertain by simply watching a video.

The sawtooth nature of jet breakup discussed in Section 3.1 is shown in Fig. 6. The dark striated pattern in the STDs represents empty space, and the slope represents jet velocity. The steeper patterns associated with an aluminum sheet in Fig. 6a correspond to a faster jet from the undilated aluminum nozzle, contrasted by the gentler slopes of the elastomer nozzles in Fig. 6b-d. The width between

dark bands corresponds to more spatial distance between proximal drops after breakup, and a jump in dark bands toward the top of the frame corresponds to the shortening of breakup distance induced by the pressure pulse.

Rayleigh-Plateau instabilities (Rayleigh 1878) in the coherent portions of the jets toward the tops of the STD frames are shown by colorful, wave-like patterns running dominantly horizontally and are mostly clearly shown in Fig. 6b and d. Further exploration of jet morphology using wave-like patterns in STDs is a fruitful area for future work. The striations are interrupted after the application of the pulse, before resuming as the jet recovers. The pulse produces a larger  $\Delta Z$  the softer material, which requires a longer time for the disturbance to reach the field of view and a longer recovery time, as shown in Fig. 6d. We interpret the longer recovery time as a direct result of a slower jet, due to dilation. However, despite the longer recovery time, the predicted We<sup>1/2</sup> $\check{D}$  value at which the pulse no longer impacts jet breakup is the lowest for the softest nozzle (Table 2). An annotated version of Fig. 6d, showcasing the features discussed above, is given in Fig. 7.

#### 4 Discussion and conclusions

Nozzle material properties are one of the dominant variables governing the stability and robustness of our liquid jets. This study seeks to set a foundation by which researchers can begin unraveling how material properties of the nozzle, such as compliance and viscoelasticity, affect the propagation and dissipation of pressure waves in the liquid jet. Our nozzles undergo significant strain due to the static pressure difference between the liquid in the relaxation chamber and the atmosphere. Prior research has shown that large finite deformations and corresponding stress states can influence wave propagation in monolithic elastomers (Bertoldi and



Experiments in Fluids (2025) 66:176 Page 9 of 11 176

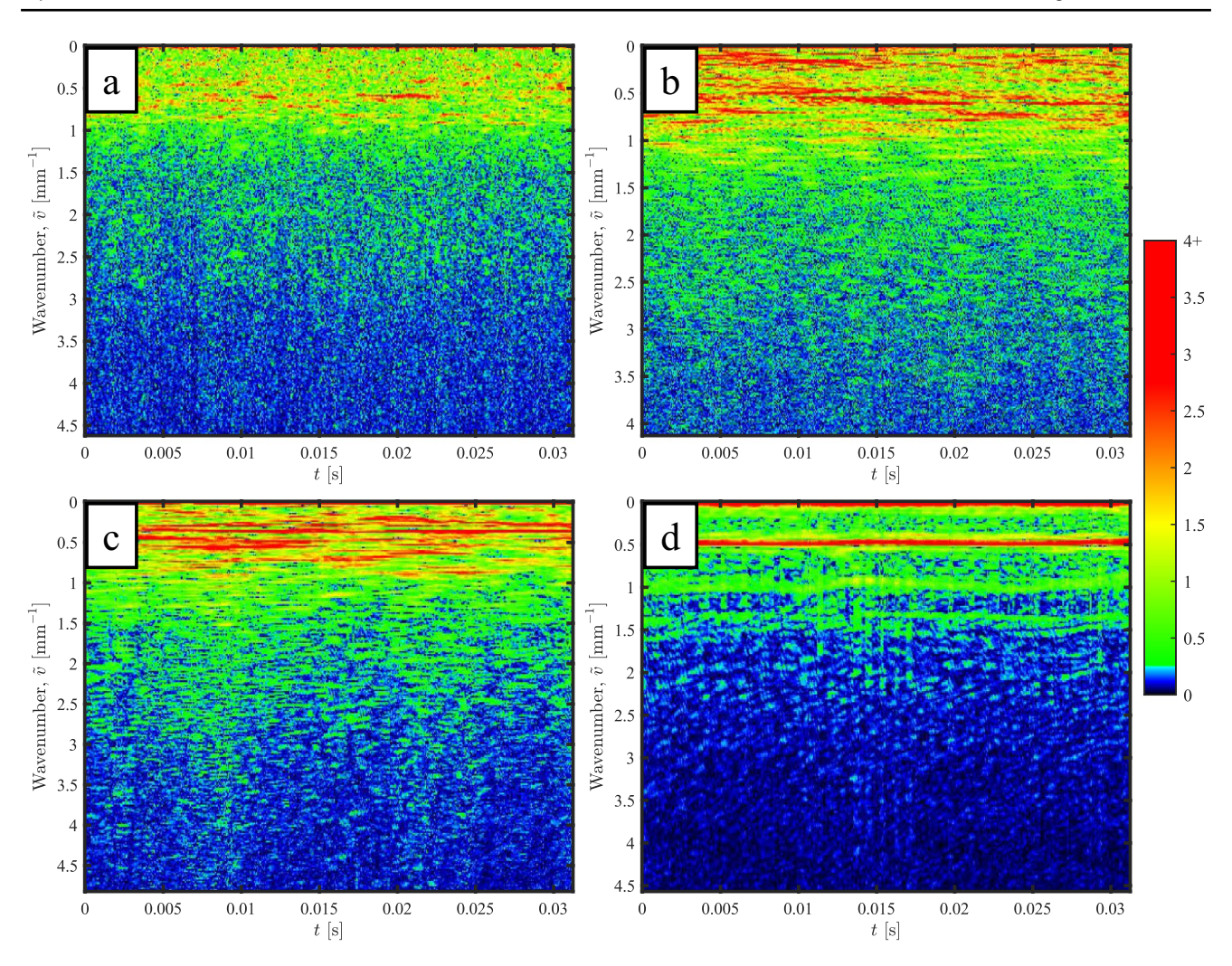


Fig. 8 Wavenumber intensity plots for (a) aluminum, (b) 35A, (c) 20A, and (d) 10A based on the viewing window of top 5 mm and t = 0 - 31.25 ms of Fig. 6. Maximum intensity values for each panel are 16, 14, 18, and 18, respectively

Boyce 2008). Both elastic instabilities and propagation of acoustic waves are strongly influenced by geometric patterns, material properties, and loading conditions. How such behavior of the nozzle material might affect the propagation and dispersion of pressure waves into the liquid jets remains an avenue of exploration for future researchers. To the authors' knowledge, we are the first to study liquid jets with elastic nozzles(Alif et al. 2023) and the first to perturb such jets with a pressure pulse. A complete answer to how the coupled jet–elastic nozzle system governs stability under various conditions will require further experimentation, computation, and collaboration.

For now, we can conclude that applying an upstream pressure pulse in our elastic nozzle system momentarily reduces jet stability and changes morphology, as shown in Figs. 5 and 6. Holding all the parameters constant, we conclude that softer nozzles produce more robust jets, i.e., jets from softer nozzles are less sensitive to upstream

disturbances. Softer nozzles allow more global deformation similar to a stiffer material with a larger 'drumhead.' However, a softer nozzle undergoes larger dilation and thus produces a more stable jet. Modulating the initial diameter of the nozzle is an avenue for exploration for future investigators. We expect the influence of a pulse of similar magnitude to ours to be more dominant for a smaller  $D_0$ —smaller jets are categorically less stable (Etzold et al. 2018).

The dominant forces involved in pulse-induced breakup are different compared to the forces of the four traditional breakup regimes mentioned in Section 1. The 'steady' jets investigated in this study reside in the Rayleigh and the first wind-induced regimes, limited by nozzle failure, but arguably the application of the pulse requires new regime definitions, similar to the regimes defined for co-flowing gases (Chigier and Farago 1992; Chigier 1996). A rigid ring concentric to the nozzle could be added to the surface of the planar membrane to cap  $\check{D}$  to a constant maximum value, allowing trials to go



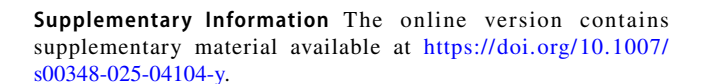
up to the predicted flow rates in Table 2 without membrane rupture. Limiting nozzle dilation would isolate the membrane contribution to jet stability from nozzle dilation and limit the size of the dollop formed after application of a pulse. As a first attempt to glean more knowledge from our STDs, we isolate the pre-breakup and pre-pulse portion of the STDs (top left) and perform an FFT such that each column in the STD is transformed into a column of wavenumber for each time step. We plot wavenumber vs time in Fig. 8 Jets from the 10A membrane show distinct wavenumber at 0.5 mm<sup>-1</sup>, corresponding to the distinct wave-like Rayleigh-Plateau instability bands seen in the top left portion of Fig. 6d. The patterns in STDs of 35A and 20A as shown in Fig. 6b,c are noisier, resulting in more sparse distributions in Fig. 8b and c. Aluminum nozzles show more random instability; thus, no distinct distributions are shown in Fig.8a.

Experimentally, we have introduced a dilating elastic planar nozzle system rife with parametric complexity. The sheer number of variables in fluid properties, nozzle materials and dimensions, and pulse domains make our system an ideal candidate to study for learning algorithms(Alam et al. 2020; Orkweha et al. 2021; Dickerson et al. 2022). Such an approach could be used to predict stability, dilation, and morphological changes to the liquid column for jet optimization toward specific applications. As alluded to in Section 3.3, there is more information embedded in the STDs of Fig. 6 than we can extract from a cursory view. Computational tools, such as learning algorithms perhaps, are capable of extending our understanding of the nature of instabilities and our predictions of their behavior.

Computational learning tools may also enable a closer look at the connection between the nature of the pressure pulse and the ensuing response. We posit that the nature of the pulse, such as magnitude, duration, and periodicity, will drive which nozzle material and geometry are best suited to dissipate the influence of the disturbance. Such an optimum choice is likely to be best chosen algorithmically, rather than theoretically. A periodic pulse may elucidate underlying resonant modes in the jet response for nozzles of various materials. These modes might be a function of the nozzle elasticity and viscoelasticity. Further insight into such behavior will allow us to build more damping capacity in a system based on expected upstream disturbances.

# 5 Supplementary Material

The supplementary material includes (i) a temporal plot of the sound pressure intensity of the pressure pulse, (ii) a detailed derivation of Eq.(1), (iii) a plot relating Q, E, and Z/D, and (iv) a movie showcasing the behavior of our jets.



**Acknowledgements** We would like to thank the National Science Foundation (CBET-2205558) for support.

Author Contributions M.E.A. designed and created the experimental setup, collected data, performed data analysis, generated all the tables, and wrote the main manuscript text. M.B. and F.M. assisted with experimental method creation and data collection. C.W. and R.B. collected data and assisted in pre- and post-processing data before and after analysis, and generated figure graphics. R.C. led material relaxation time measurements. A.K.D. supervised the project, assisted with experimental design, reviewed data, and wrote and edited the manuscript.

**Data Availability** Raw experimental videos and data are publicly available in perpetuity via OneDrive. Interested parties should contact the corresponding author for access.

### **Declarations**

**Conflict of interest** The authors declare no conflict of interest.

#### References

- Alam ME, Wu D, Dickerson AK (2020) Predictive modelling of drop ejection from damped, dampened wings by machine learning. Proc R Soc A 476:20200467
- Alif ME, Veihdeffer J, Alam ME, Dickerson AK (2023) Liquid jet stability through elastic planar nozzles. Europ Phys J Special Top 232:827–835
- Amini G, Dolatabadi A (2011) Capillary instability of elliptic liquid jets. Phys Fluids 23:084109
- Amini G, Dolatabadi A (2012) Axis-switching and breakup of lowspeed elliptic liquid jets. Int J Multiph Flow 42:96–103
- Amini G, Lv Y, Dolatabadi A, Ihme M (2014) Instability of elliptic liquid jets: temporal linear stability theory and experimental analysis. Phys Fluids 26:114105
- Ashgriz N (ed) (2011) Handbook of atomization and sprays: theory and applications. Springer Science & Business Media
- Ashgriz N, Yarin A (2011) Capillary instability of free liquid jets. In Handbook of Atomization and Sprays, pp. 3–53. Springer
- Bertoldi K, Boyce MC (2008) Wave propagation and instabilities in monolithic and periodically structured elastomeric materials undergoing large deformations. Phys Rev B 78:184107. https://doi.org/10.1103/PhysRevB.78.184107
- Bidone G (1829) Expériences sur la forme et sur la direction des veines et des courans d'eau lancés par diverses ouvertures. De l'Imprimerie royale, Par Georges Bidone
- Blaisot J, Adeline S (2003) Instabilities on a free falling jet under an internal flow breakup mode regime. Int J Multiph Flow 29:629-653
- Carter JC, Alvis RM, Brown SB, Langry KC, Wilson TS, McBride MT, Myrick M, Cox WR, Grove ME, Colston BW (2006) Fabricating optical fiber imaging sensors using inkjet printing technology: a pH sensor proof-of-concept. Biosens Bioelectron 21:1359–1364
- Chigier N (1996) Regimes of jet breakup and breakup mechanisms (physical aspects). Prog Astronaut Aeronaut 166:109–134



Experiments in Fluids (2025) 66:176 Page 11 of 11 176

Chigier N, Farago Z (1992) Morphological classification of disintegration of round liquid jets in a coaxial air stream. Atomization and sprays. 2

- Couty P, Spiegel A, Vágó N, Ugurtas B, Hoffmann P (2004) Laser-induced break-up of water jet waveguide. Exp Fluids 36:919-927
- Dickerson AK, Alam M, Buckelew J, Boyum N, Turgut D (2022) Predictive modeling of drop impact force on concave targets. Physics of Fluids. 34
- Eggers J, Villermaux E (2008) Physics of liquid jets. Rep Prog Phys 71:036601
- Entov V, Yarin A (1980) Dynamical equations for a liquid jet. Fluid Dvn 15:644–649
- Entov V, Yarin A (1984) The dynamics of thin liquid jets in air. J Fluid Mech 140:91–111
- Eroglu H, Chigier N, Farago Z (1991) Coaxial atomizer liquid intact lengths. Phys Fluids A 3:303–308
- Etzold M, Deswal A, Chen L, Durst F (2018) Break-up length of liquid jets produced by short nozzles. Int J Multiph Flow 99:397–407
- Furlani EP, Price BG, Hawkins G, Lopez AG (2006) Thermally induced marangoni instability of liquid microjets with application to continuous inkjet printing. In Proc. NSTI nanotechnology conference, pp. 534–537
- Gañán-Calvo A, Barrero A (1999) A novel pneumatic technique to generate steady capillary microjets. J Aerosol Sci 30:117–125
- Ghassemieh E, Versteeg HK, Acar M (2006) The effect of nozzle geometry on the flow characteristics of small water jets. Proc Inst Mech Eng C J Mech Eng Sci 220:1739–1753. https://doi.org/10.1243/0954406imes430
- Guha A, Barron R, Balachandar R (2011) An experimental and numerical study of water jet cleaning process. J Mater Process Technol 211:610–618
- Jarrahbashi D, Sirignano WA (2012) Acceleration effects on instability of high-pressure fuel jets. In Proceedings of the Twelfth international conference on liquid atomisation and spray systems (ICLASS), pp. 1–8
- Kalaaji A, Lopez B, Attane P, Soucemarianadin A (2003) Breakup length of forced liquid jets. Phys Fluids 15:2469–2479
- Krsmanovic M, Biswas D, Ali H, Kumar A, Ghosh R, Dickerson AK (2021) Hydrodynamics and surface properties influence biofilm proliferation. Adv Coll Interface Sci 288:102336
- Larson K (2016) Can you estimate modulus from durometer hardness for silicones? Technical report, Dow Corning Coroporation
- Lefebvre AH, McDonell VG (2017) Atomization and Sprays. CRC Press
- Lin S, Reitz R (1998) Drop and spray formation from a liquid jet. Annu Rev Fluid Mech 30:85–105
- MacFarlane D, Narayan V, Tatum J, Cox W, Chen T, Hayes D (1994) Microjet fabrication of microlens arrays. IEEE Photonics Technol Lett 6:1112–1114
- Menezes V, Kumar S, Takayama K (2009) Shock wave driven liquid microjets for drug delivery. Phys Fluids 106:086102
- Mitragotri S (2006) Current status and future prospects of needle-free liquid jet injectors. Nat Rev Drug Discov 5:543–548
- Ohnesorge WV (1936) Formation of drops by nozzles and the breakup of liquid jets. Z Angew Math Mech 16:355–358
- Orkweha P, Downing A, Lebanoff AP, Zehtabian S, Bacanli SS, Turgut D, Dickerson AK (2021) Ensemble machine learning predicts displacement of cantilevered fibers impacted by falling drops. J Fluids Struct 102:103253

- Rajesh K, Sakthikumar R, Sivakumar D (2016) Interfacial oscillation of liquid jets discharging from non-circular orifices. Int J Multiph Flow 87:1–8
- Ranz W (1956) On sprays and spraying. Pennsylvania State University Bulletin, Department of Engineering Research
- Rayleigh L (1878) On the instability of jets. Proc Lond Math Soc 1:4–13
- Rayleigh L (1879) On the capillary phenomena of jets. Proc R Soc London 29:71–97
- Reneker DH, Yarin AL, Fong H, Koombhongse S (2000) Bending instability of electrically charged liquid jets of polymer solutions in electrospinning. J Appl Phys 87:4531–4547
- Savart F (1833) Memoire sur la constitution des veines liquides lancees par des orifices circulaires en mince paroi. Anal Chem 53:337–386
- Schoppink JJ, Mohan K, Quetzeri-Santiago MA, McKinley G, Rivas DF, Dickerson AK (2023) Cavitation-induced microjets tuned by channels with alternating wettability patterns. Phys Fluids 35:032017
- Sirignano W, Mehring C (2000) Review of theory of distortion and disintegration of liquid streams. Prog Energy Combust Sci 26:609–655
- Smith NM, Ebrahimi H, Ghosh R, Dickerson AK (2018) High-speed microjets issue from bursting oil gland reservoirs of citrus fruit. Proc Natl Acad Sci 115:E5887–E5895
- Song Y, Hwang D, Ahn K (2017) Effect of orifice geometry on spray characteristics of liquid jet in cross flow. In 55th AIAA Aerospace Sciences Meeting, p. 1961
- Sterling AM, Sleicher C (1975) The instability of capillary jets. J Fluid Mech 68:477–495
- Tagawa Y, Oudalov N, El Ghalbzouri A, Sun C, Lohse D (2013) Needle-free injection into skin and soft matter with highly focused microjets. Lab Chip 13:1357–1363
- Varga CM, Lasheras JC, Hopfinger EJ (2003) Initial breakup of a small-diameter liquid jet by a high-speed gas stream. J Fluid Mech 497:405–434
- Wang F, Fang T (2015) Liquid jet breakup for non-circular orifices under low pressures. Int J Multiph Flow 72:248–262
- Zhang Y-P, Lee S-H, Reddy KR, Gopalan AI, Lee K-P (2007) Synthesis and characterization of core-shell SiO<sub>2</sub> nanoparticles/poly (3-aminophenylboronic acid) composites. J Appl Polym Sci 104:2743–2750
- Zhao Y, Wan D, Chen X, Chao X, Xu H (2021) Uniform breaking of liquid-jets by modulated laser heating. Physics of Fluids. 33
- Zhou J, Andersson M (2020) An analysis of surface breakup induced by laser-generated cavitation bubbles in a turbulent liquid jet. Exp Fluids 61:1–19

**Publisher's Note** Springer Nature remains neutral with regard to jurisdictional claims in published maps and institutional affiliations.

Springer Nature or its licensor (e.g. a society or other partner) holds exclusive rights to this article under a publishing agreement with the author(s) or other rightsholder(s); author self-archiving of the accepted manuscript version of this article is solely governed by the terms of such publishing agreement and applicable law.

